Functionalization of iron oxide magnetic nanoparticles with poly(methyl methacrylate) brushes via grafting-from atom transfer radical polymerization

ARTICLE *in* JOURNAL OF POLYMER SCIENCE PART A POLYMER CHEMISTRY · MARCH 2007

Impact Factor: 3.11 · DOI: 10.1002/pola.21854

Functionalization of Iron Oxide Magnetic Nanoparticles with Poly(methyl methacrylate) Brushes Via Grafting-From Atom Transfer Radical Polymerization

I. GARCIA,[1] N. E. ZAFEIROPOULOS,[2] A. JANKE,[2] A. TERCJAK,[1] A. ECEIZA,[1] M. STAMM,[2] I. MONDRAGON[1]

[1]Materials and Technologies Group, Departamento Ingeniería Química y Medio Ambiente, Escuela Politécnica, Universidad País Vasco/Euskal Herriko Unibertsitatea, Plaza Europa 1, 20018 Donostia-San Sebastián, Spain

[2]Department of Nanostructured Materials, Leibniz Institut für Polymerforschung Dresden, Hohe Strasse 6, D-01069 Dresden, Germany

Received 8 September 2006; accepted 23 October 2006
DOI: 10.1002/pola.21854
Published online in Wiley InterScience (www.interscience.wiley.com).

ABSTRACT: A key problem with nanomaterials is the difficulty of controlling the dispersion of nanoparticles inside an organic medium. To overcome this problem, functionalization of the nanoparticle surface is required. Poly(methyl methacrylate) (PMMA) brushes were grown on the surface of iron oxide magnetic nanoparticles with atom transfer radical polymerization and a grafting-from approach. Modified magnetic nanoparticles with a graft density of 0.1 PMMA chains/nm^2 were obtained. Cu(II), used as a deactivating complex, allowed good control of the polymerization along with a narrow polydispersity of the polymer chains. The functionalized magnetic nanoparticles were characterized with Fourier transform infrared spectroscopy, thermogravimetric analysis, gel permeation chromatography, and atomic force microscopy. © 2007 Wiley Periodicals, Inc. J Polym Sci Part A: Polym Chem 45: 925–932, 2007
Keywords: atomic force microscopy (AFM); atom transfer radical polymerization (ATRP); FT-IR; graft polymerization; magnetic nanoparticles

INTRODUCTION

Magnetic nanoparticles (MNs) have been a subject of extensive research because of their potential applications in many diverse fields, such as magnetic ferrofluids, contrast agents for magnetic resonance imaging, biomedical materials, catalysis, and MN/ligand targeting systems for drug delivery.[1–4] In recent years, nanomaterials have received increasing interest as potential candidates to replace traditional materials because novel materials can be obtained with a unique combination of properties at lower filler weight fractions in comparison with traditional composites with microsize fillers.[5] One significant problem, however, with nanomaterials is the difficulty of controlling the dispersion of nanoparticles inside an organic medium. To overcome this problem, it is often necessary to functionalize the nanoparticles and hence ensure effective control of the dispersion.[6,7]

For the preparation of organic/inorganic hybrid materials consisting of an organic polymer and inorganic nanoparticles, different chemical methods have been proposed to attach a polymer to a surface. The first method is known as *grafting-to*: polymers with suitable end-functional groups react with appropriate surface sites on the inorganic nanoparticles.[8–10] The second method is a surface copolymerization through a covalently linked mono-

Correspondence to: I. Mondragon (E-mail: inaki.mondragon@ehu.es)

mer, and in this route, the inorganic phase is incorporated inside the polymer chains.[11,12] In the third method, known as *grafting-from*, chains grow *in situ* from initiator molecules that have been pregrafted onto the surface of the nanoparticles.[9–15] This technique, combined with controlled radical polymerization (CRP), has been used to build up highly dense polymer brushes on planar surfaces[16] and recently has also been extended to nanoparticles to functionalize them.[17] Recent advances in CRP have allowed us to obtain polymer brushes with good control of the molecular weight and polydispersity (PI). There are different CRP methods that allow us to grow brushes on the surfaces of nanoparticles. CRP has a different feature with respect to other methods of polymer synthesis, the difference being the existence of an equilibrium between active and dormant species, and because of this, good control over the molecular weight can be obtained. Different methods of living radical polymerization, such as atom transfer radical polymerization (ATRP), reversible addition–fragmentation chain transfer, and nitroxide-mediated polymerization (NMP), exist.[18–20] One of the most common CRPs used to create polymer brushes is ATRP, in which an atom transfer step is the key elementary reaction responsible for the uniform growth of the polymer chains.[21] ATRP allows us to create brushes on surfaces consisting of the generation of radicals by a reversible redox equilibrium in which a halogen is transferred from the deactivated chain end to a metal halide catalyst. In the synthesis of controlled brushes by ATRP, two techniques can be applied. In the first method, a sacrificial free initiator is used, whereas in the second method, a persistent radical should be added, to set up the equilibrium and thereby lead to controlled polymerization.

Polymer chains have been grafted onto silicon surfaces or nanoparticles, and this has led to a range of graft densities.[22–24] Moreover, poly (methyl methacrylate) (PMMA) brushes have been synthesized by ATRP onto gold nanoparticles[25] with a graft density 0.3 chains/nm^2. NMP was used by Matsuno et al.[26] for modifying iron oxide nanoparticles with polystyrene and poly(3-vinylpyridine), who obtained a graft density between 0.12 and 0.2 chains/nm^2. In this work, PMMA brushes were grown on iron oxide MNs by ATRP (Scheme 1); the elementary reaction of this polymerization, the transfer step, was responsible for the growth of the polymer chains. In this study, iron oxides were functionalized with PMMA brushes with ATRP. The resultant materials were characterized with Fourier transform infrared (FTIR) spectroscopy, thermogravimetric analysis (TGA), gel permeation chromatography (GPC), and atomic force microscopy (AFM).

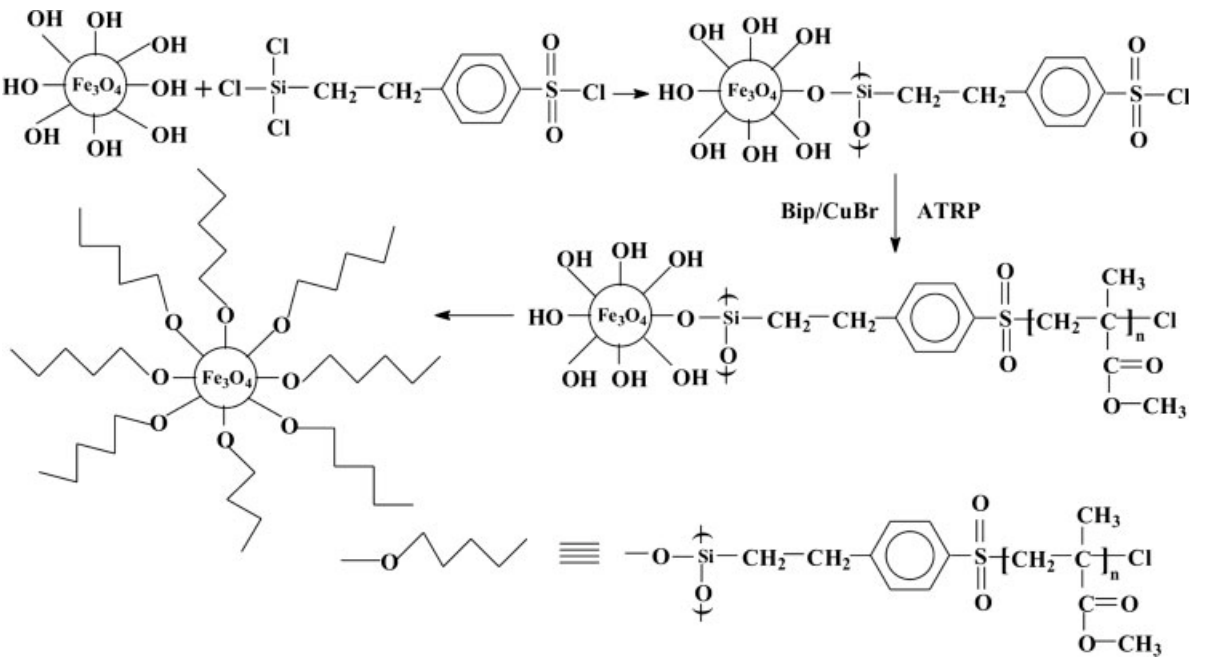

Scheme 1. ATRP procedure for growing PMMA brushes on nanoparticles.

EXPERIMENTAL

The modification of nanoparticles with PMMA brushes was performed in two steps. First, 2-(4-chlorosulfonylphenyl)ethyltrichlorosilane (CTCS) as an initiator was anchored onto MNs. Second, the ATRP of PMMA was carried out with copper bromide (CuBr)/2,2′-bipyridine (Bip) as a catalyst system.

Materials

Magnetite (Fe_3O_4) nanoparticles with a nominal size of 9 nm and a PI of 1.34 were purchased from Integran Technologies, Inc.[27] (Canada), and used as received. The monomer methyl methacrylate (MMA; 99%) was purchased from Aldrich (Germany) and was distilled under reduced pressure over CaH_2 before use. CTCS was purchased from ABCR (Germany) and used in the form of a 50 wt % solution in dichloromethane containing 30% free sulfonic acid and small amounts of silylsulfonic acid without any further purification. CuBr (98.0%), copper(II) bromide ($CuBr_2$; 99.9%), and Bip (99.0%) were purchased from Aldrich (Germany) and used as received. An aqueous hydrochloric acid (HCl) solution (37%) and *p*-toluenesulfonylchloride (TsCl) were purchased from Fluka and used as received. Finally, extradry toluene was purchased from Acros and used without any further purification as well.

Surface Deposition of the Initiator on MNs

Pioneering work for the use of sulfonyl chloride initiators in ATRP was carried out by Percec and coworkers.[28] In this work, the immobilization of the CTCS initiator on the MN surfaces was carried out with the procedure of Marutani et al.[29] Extradry toluene, CTCS, and MNs were mixed in an ultrasonic bath at room temperature. The MNs were subsequently washed six times with tetrahydrofuran (THF) and then dried *in vacuo* at 40 °C for a period of 2 days.

ATRP Polymerization of PMMA on MNs

The polymerization of PMMA was performed with CuBr/Bip as the catalyst[30] and with CTCS on MNs as the initiator. A solution that contained deoxygenated MMA (32.16 g, 319.88 mmol), CuBr (15.89 mg, 0.16 mmol), $CuBr_2$ (1.78 mg, 0.008 mmol), Bip (78.7 mg, 0.504 mmol), and 0.500 g of CTCS–MNs was sealed under a nitrogen atmosphere and heated at 70 °C for 5 h.

ATRP Bulk Polymerization of Neat PMMA

The bulk polymerization of neat PMMA was performed under the same conditions used in the polymerization of PMMA on the MN surfaces, but without the presence of nanoparticles and with TsCl as the initiator. The reaction was carried out at 70 °C for 90 min.

Cleavage of PMMA Brushes from the MN Surface

The grafted PMMA was cleaved from the surface of the nanoparticles with the method described by Matsuno et al.[31] HCl was used to dissolve the iron oxide nanoparticles. Subsequently, a small part of the isolated polymer was analyzed with GPC.

Characterization of the Modified Nanoparticles

Brunauer–Emmett–Teller (BET) isotherms were obtained with an Autosorb-1 from Quantachrome (United States). The samples were dried at 100 °C for 2 h in a vacuum oven. Nitrogen was used as the adsorbent, and all measurements took place at −196 °C.

FTIR spectra were recorded with a FTIR spectrometer (IFS66v, Bruker). The nanoparticles were pressed together with KBr to form pellets, which were analyzed via the signal averaging of 32 scans at a resolution of 2 cm^{-1}. Blind measurements of neat KBr were also obtained and subtracted from the final spectra.

TGA was performed with a TA Instrument TGA Q500 under a nitrogen atmosphere at a heating rate of 10 °C/min from room temperature to 600 °C.

The molecular weight and molecular weight distribution were determined by GPC with a Perkin-Elmer chromatograph equipped with a binary pump and a refractive-index detector. The mobile phase was THF, and the separation was carried out with three Styragel columns packed with 5-μm particle gel with nominal pore sizes of 100, 500, and 10^4 Å and with an elution rate of 1 mL/min at 30 °C. The columns were calibrated with polystyrene standards before the measurements according to standard procedures. The GPC results are expressed as polystyrene-equivalent molecular weights. The system was interfaced to a personal computer equipped with Turbochrom Workstation software for data collection and handling.

AFM measurements were performed in the tapping mode with a Dimension 3100 NanoScope IV (Veeco, United States). We used silicon Scanning Probe Microscopy (SPM) sensors (Budget-

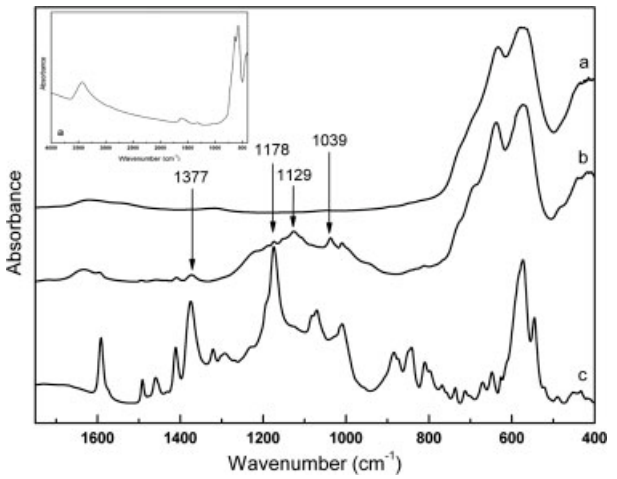

Figure 1. FTIR spectra of (a) MNs, (b) CTCS–MNs, and (c) CTCS.

Sensors, Bulgaria) with a spring constant of about 3 N/m and a resonance frequency of about 75 kHz; the tip radius was lower than 10 nm. The images on the left show the surface morphology, and those on the right are the simultaneously taken phase images. According to Magonov et al.,[32] we chose the scan conditions (free amplitude $>$ 100 nm, set-point amplitude ratio $=$ 0.5) to get a stiffness contrast in the phase image; this means that the bright features in the phase image are stiffer than the dark areas.

RESULTS AND DISCUSSION

Characterization of the MNs

The specific surface area of the MNs measured with the BET method was estimated to be 123 m^2/g. The quantity of hydroxyl groups on the MN surfaces was determined with the use of TGA according to the method of Abbound et al.[33] The surface density of the hydroxyl groups was found to be 8.5 OH/nm^2.

A typical FTIR spectrum of the MNs is shown in Figure 1. The peak around 3400 cm^{-1} can be attributed to OH bonds of the MN hydroxyl groups. The other two peaks at 637 and 572 cm^{-1} are due to the Fe—O bond.[34,35] As can be easily seen, there is a complete absence of any carbon-related peaks, and this shows that the neat MNs were surfactant-free.

Immobilization of CTCS on MNs

The introduction of CTCS onto MNs is of pivotal importance for further grafting from the MN surface because the sulfonyl chloride groups of the compound will control the growth of PMMA chains on the MN surface. After the modification of the MN surface with CTCS, the amount of the grafted initiator was determined by TGA.[36] The surface density of the initiator was about 1.5 molecules/nm^2. A direct comparison of the surface density of the hydroxyl groups and that of the initiator on the MN surface yielded a reaction efficiency of 18.5%. The reaction between hydroxyl groups of the MNs and CTCS was also confirmed with FTIR (Fig. 1). Two new peaks at 1039 and 1129 cm^{-1} in the CTCS–MN spectrum are evident. The first peak can be attributed to the formation of new Si—O—Si bonds ($\nu_{Si-O-Si}$ = 1039 cm^{-1}) as the trichlorosilane groups underwent a self-condensation reaction to form a polysiloxane film on the iron oxide surface.[37] The second peak (ν_{Si-O} 1129 cm^{-1}) can be attributed to the MN—O—Si bond that was created between MNs and CTCS after the reaction. The other peaks observed in both spectra can be assigned to the symmetric stretching of the S=O bond ($\nu_{S=O}$ = 1377 cm^{-1}), and to the asymmetric stretching of the S=O bond (ν_{S-O} = 1178 cm^{-1}) of CTCS. These experimental findings strongly suggest that CTCS indeed reacted with the surface OH groups.

Polymerization of PMMA on CTCS–MNs

The CTCS–MNs were subjected to ATRP, in which Cu(II) was used to obtain a satisfactory result for the control of polymerization because its addition as a radical deactivator at the beginning of the reaction facilitated exchange reactions between

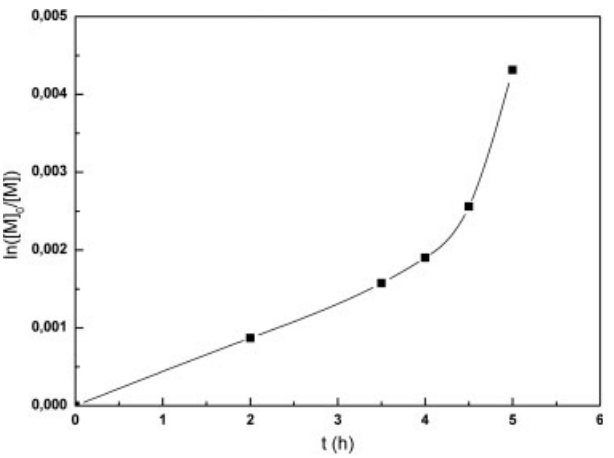

Figure 2. Plot of $\ln([M]_0/[M])$ versus reaction time t for the solution polymerization of MMA at 70 °C with CTCS–MNs as the initiator.

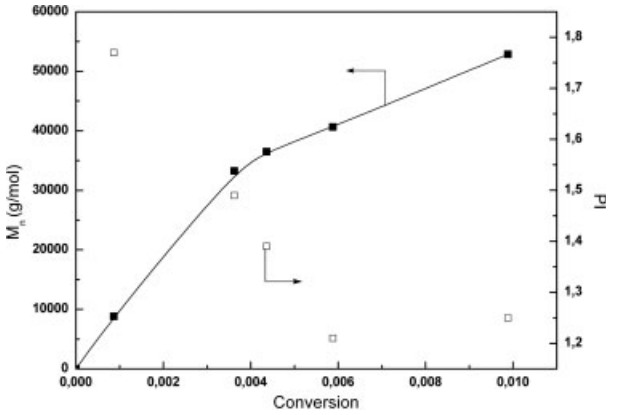

Figure 3. Plot of M_n and PI versus the conversion for the solution polymerization of MMA at 70 °C with CTCS–MNs as the initiator.

the active radicals and dormant oligomeric/polymeric halides.[38,39]

Figure 2 shows a plot of the degree of conversion, $\ln([M]_0/[M])$, versus the reaction time for the polymerization of MMA in bulk with CTCS–MNs, where $[M]_0$ and [M] are the initial and nonreacted monomer concentrations, respectively. The polymerization has first-order kinetics until 4 h of reaction. Thereafter, the plot is upward and concave with increasing polymerization time. As reported by Sumerlin et al.,[40] who showed that only a few polymer chains are necessary to induce gelation in ATRP, this nonlinearity may come from the high increase in the system viscosity.[41] To corroborate this point, the polymer cleaved from PMMA–MNs at several reaction times was analyzed with GPC. Figure 3 shows the number-average molecular weight (M_n) and PI evolution throughout the reaction. The degree of conversion was calculated with TGA. This nonlinear curve corresponds to the typical behavior for systems in which initiation with respect to propagation is slow. The deviation of the molecular weight from the linear theoretical behavior can be attributed to steric congestion, which generates an increase in the system viscosity because of the gel effect provoked by interparticle radical coupling.[42] Indeed, the GPC results showed a narrow PI[42] instead of a bimodal distribution of molecular weights cleaved from MNs.

Figure 4 shows the linear relationship of $\ln([M]_0/[M])$ versus the reaction time for the bulk polymerization of MMA under the same stoichiometric ratio of polymerization, only changing the colloidal initiator to TsCl, which is a molecular initiator similar to CTCS. In comparison with the results obtained in the polymerization with CTCS–MNs, a lower rate of polymerization can be observed, these results being similar to those obtained by Pyun et al.[42]

The grafting density of PMMA anchored to MNs was calculated with the method proposed by Ohno et al.[25] The grafting density was nearly constant, independent of the time, and approximately equal to 0.1 chains/nm^2. This low efficiency of the initiator anchored to MNs could be due to steric congestion of the initiator on the surface[42] or to termination reactions between the growing radical and a surface-bound polymer chain.[35]

Figure 5 shows FTIR spectra of PMMA, CTCS–MNs mixed with PMMA (CTCS–MNs+PMMA), CTCS–MNs, and MNs modified with PMMA (PMMA–MNs). The modification of CTCS–MNs

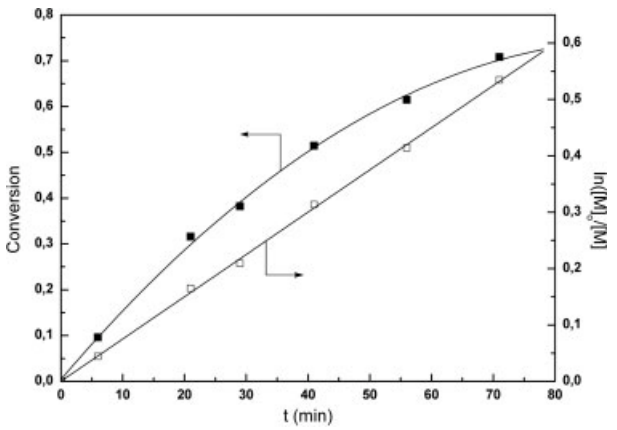

Figure 4. Plot of the conversion and $\ln([M]_0/[M])$ versus reaction time t for the solution polymerization of MMA at 70 °C with TsCl as the initiator.

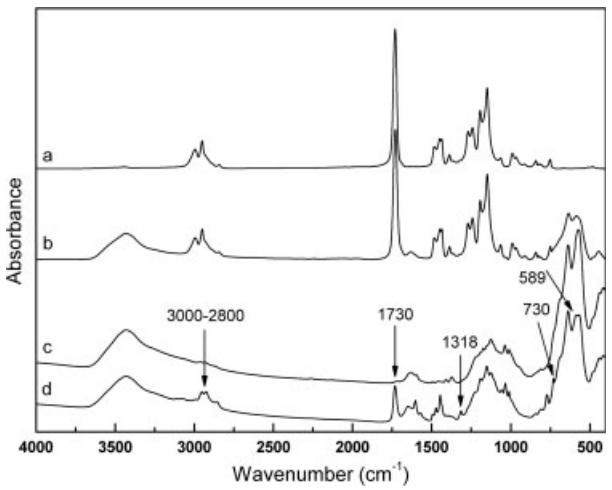

Figure 5. FTIR spectra of (a) PMMA, (b) CTCS–MNs+PMMA, (c) CTCS–MNs, and (d) PMMA–MNs.

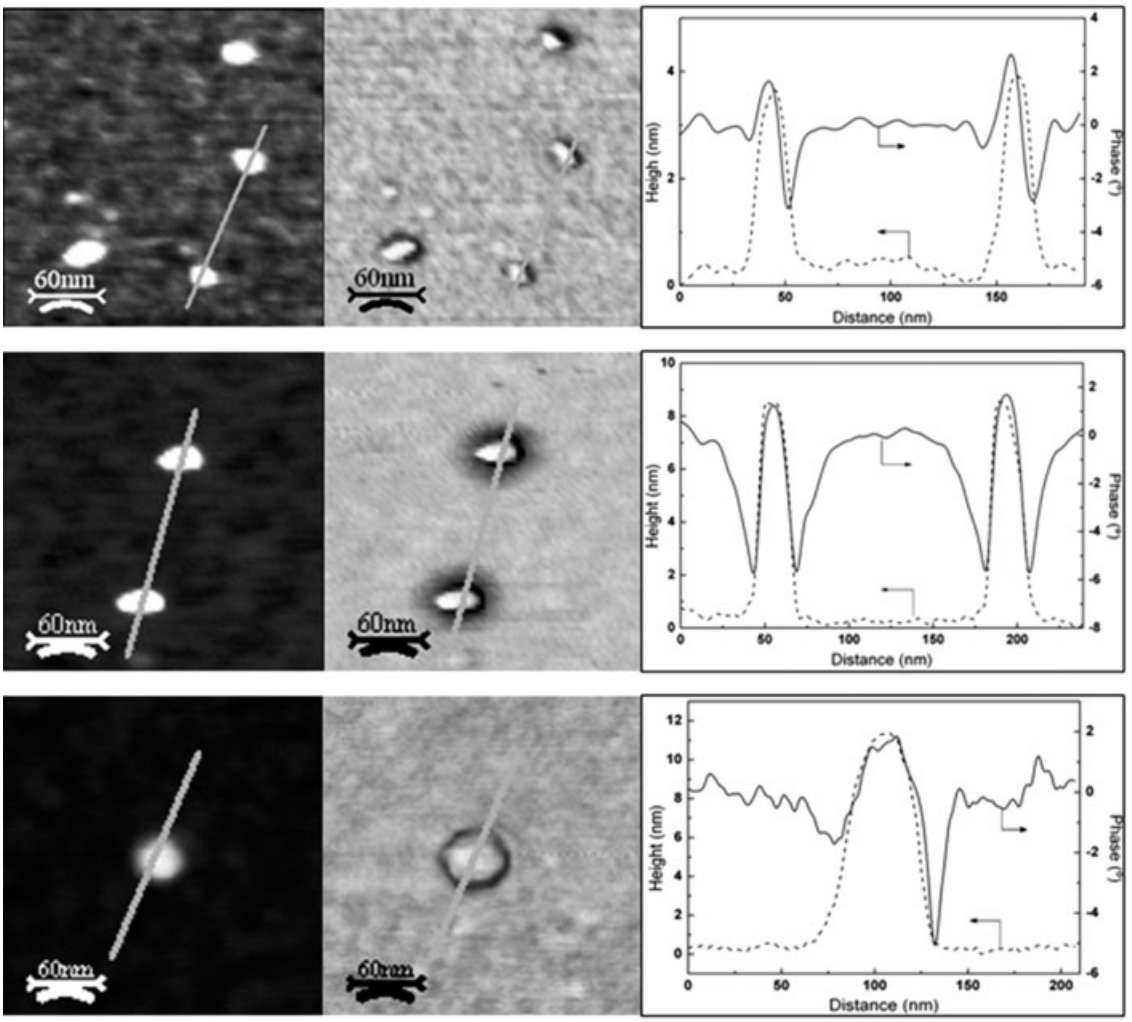

Figure 6. Height (left) and phase (center) AFM images and height and phase profiles (right) of unmodified MNs (top), PMMA–MNs (center), and PMMA–MNs after a thermal treatment at 500 °C (bottom).

with PMMA was confirmed by a new peak at 1730 cm^{-1} attributed to the ester group of PMMA.

Comparing CTCS–MNs and PMMA–MNs, we also observed a displacement of the S=O bond due to the influence of neighboring groups. The position for this group in Ar—SO_2—Cl ($\nu_{S=O}$ = 1377 cm^{-1}) is different from the position in Ar—SO_2—R ($\nu_{S=O}$ = 1318 cm^{-1}). Spectra of CTCS–MN+PMMA and PMMA–MNs were compared, and a new peak was observed, which could be attributed to the stretching of S—C (ν_{S-C} = 730 cm^{-1}). This band strongly indicates that MNs are not coated by PMMA, but PMMA is grafted on the MN surface. A new peak observed at 589 cm^{-1} for PMMA–MNs could be attributed to the deformation of the SO group. A high increase in the characteristic stretching bands of the aliphatic chains at 2800–3000 cm^{-1} was observed for PMMA–MNs.

Representative AFM images are shown in Figure 6. Samples were prepared through the solvent evaporation of very diluted dispersions of MNs, PMMA–MNs, and PMMA–MNs that underwent a thermal treatment at 500 °C for 6 h to degrade PMMA (DPMMA–MNs) on silicon wafers. In the height/phase profiles, differences between the apparent particle diameter and height can be observed. This fact can be attributed to the tip geometry smearing effect.[43–45] For this reason, the real size of the MNs was measured with the estimated height rather than lateral lengths from the height images. Comparing the phase profiles of MNs, PMMA–MNs, and DPMMA–MNs, we ob-

served changes depending on the thermal treatment to which the MNs were submitted. MNs and DPMMA–MNs showed the same behavior when analyzed with AFM. In both cases, on the phase profile, there is a change that is attributable to the phase shift due to the lateral contact between the tip and particles. In the phase image of PMMA–MNs, a different behavior around the nanoparticles can be observed. The darker, 10–20-nm-wide rings indicate softer material, which can be attributed to PMMA brushes linked to the MNs.

CONCLUSIONS

PMMA brushes were grown on the surface of commercial magnetite nanoparticle powders with the grafting-from technique by ATRP. A CuBr/Bip catalyst system and a CTCS silane for the initiation of ATRP on the surface of the nanoparticles were used. Good control of the polymerization coupled with a narrow PI of the polymer chains was achieved. A technique for introducing the initiator onto MNs was performed, unlike neat PMMA graft polymerization. The MN modification had first-order kinetics in the first steps of the reaction; thereafter, a gel effect occurred. The functionalized nanoparticles were characterized with GPC, FTIR, and TGA techniques. Brushes of PMMA with a graft density of 0.1 chains/nm^2 were anchored onto nanoparticles surface and not coated on them. AFM studies showed a corona of PMMA brushes on the functionalized nanoparticles.

This work was supported by the Nanofun-Poly Network of Excellence, the European Union Research Training Network Nanobuilding Blocks project (contract no. HPRN-CT-2002-00306), and Gobierno Vasco/Eusko Jaurlaritza (through the Etortek-Nanotron project). The authors thank D. Voigt for the gel permeation chromatography measurements, G. Adam for the Fourier transform infrared measurements, R. Häßler for the thermogravimetric analysis measurements, and V. Albrecht for the Brunauer–Emmett–Teller measurements.

REFERENCES AND NOTES

1. Zanchet, D.; Michel, C. M.; Parak, W. J.; Gerion, D.; Williams, C.; Alivisatos, P. J Phys Chem B 2002, 106, 11758–11763.
2. Kondo, A.; Fukuda, H. Colloids Surf A 1999, 153, 435–438.
3. Hsiao, J.; Taic, M.; Leed, Y.; Yanga, C.; Wangd, H.; Liua, H.; Fange, J.; Chenf, S. J Magn Magn Mater 2006, 304, e4–e6.
4. Shen, H.; Long, D.; Zhu, L.; Li, X.; Dong, Y.; Jia, N.; Zhou, H.; Xin, X.; Sun, Y. Biophys Chem 2006, 122, 1–4.
5. Ash, B.; Siegel, R.; Schadler, L. S. Macromolecules 2004, 37, 1358–1369.
6. Nikiforov, M. P.; Chernysheva, M. V.; Eliseev, A. A.; Lukashin, A. V.; Tretyakov, Y. D.; Maksimov, Y. V.; Suzdalev, I. P.; Goernert, P. Mater Sci Eng B 2004, 109, 226–231.
7. Ionov, L.; Zdyrko, B.; Sidorenko, A.; Minko, S.; Klep, V.; Luzinov, I.; Stamm, M. Macromol Rapid Commun 2004, 25, 360–365.
8. Minko, S.; Patil, S.; Datsyuk, V.; Simon, F.; Eichchorn, K.; Motornov, M.; Usov, D.; Tokarev, I.; Stamm, M. Langmuir 2002, 18, 289–296.
9. Synytska, A.; Ionov, L.; Minko, S.; Motornov, M.; Elchhorn, K.; Stamm, M.; Grundke, K. Polym Mater Sci Eng 2004, 90, 624–625.
10. Minko, S.; Muller, M.; Motornov, M.; Nitschke, M.; Grundke, K.; Stamm, M. J Am Chem Soc 2003, 125, 3896–3900.
11. Rozes, L.; Fornasieri, G.; Trabelsi, S.; Creton, C.; Zafeiropoulos, N. E.; Stamm, M.; Sanchez, C. Prog Solid State Chem 2005, 33, 127–135.
12. Trabelsi, S.; Janke, A.; Häßler, R.; Zafeiropoulos, N. E.; Stamm, M.; Fornasieri, G.; Bocchini, S.; Rozes, L.; Gerard, J.-F.; Sanchez, C. Macromolecules 2005, 38, 6068–6078.
13. Boyes, S. G.; Brittain, W. J.; Weng, X.; Cheng, S. Z. D. Macromolecules 2002, 35 4960–4967.
14. Pyun, J.; Matyjaszewski, K. Chem Mater 2001, 13, 3436–3448.
15. Carrot, G.; Diamanti, S.; Manuszak, M.; Charleux, B.; Vairon, J.-P. J Polym Sci Part A: Polym Chem 2001, 39, 4294–4301.
16. Ejaz, M.; Yamamoto, S.; Ohno, K.; Tsujii, Y.; Fukuda, T. Macromolecules 1998, 31, 5934–5936.
17. Bartholome, E.; Beyou, E.; Bourgeat-Lami, E.; Chaumont, P.; Zydowicz, N. Macromolecules 2003, 36, 7946–7952.
18. Kim, D. J.; Heo, J. Y.; Kim, K. S.; Choi, I. S. Macromol Rapid Commun 2003, 24, 517–521.
19. Xu, F. J.; Song, Y.; Cheng, Z. P.; Cheng, X. L.; Zhu, X. L.; Zhu, C. X.; Kang, E. T.; Neoh, G. Macromolecules 2005, 38, 6254–6258.
20. Xu, G.; Wu, W.; Wang, Y.; Pang, W.; Zhu, Q.; Wang, P.; You, Y. Polymer 2006, 47, 5909–5918.
21. Ninjbadgar, T.; Yamamoto, S.; Fukuda, T. Solid State Sci 2004, 6, 879–885.
22. Zhao, B. Langmuir 2004, 20, 11748–11755.
23. Devaux, C.; Chapel, J. P.; Chaumont, P. Eur Phys J E 2002, 7, 345–352.
24. Kasseh, A.; Ait-Kadi, A.; Riedl, B.; Pierson, J. F. Polymer 2003, 44, 1367–1375.
25. Ohno, K.; Koh, K.; Tsujii, Y.; Fukuda, T. Macromolecules 2002, 35, 8989–8993.

26. Matsuno, R.; Yamamoto, K.; Otsuka, H.; Takahara, A. Macromolecules 2004, 37, 2203–2209.
27. www.integran.com.
28. (a) Percec, V.; Barboiu, B. Macromolecules 1995, 28, 7970–7972; (b) Percec, V.; Grigoras, C. J Polym Sci Part A: Polym Chem 2005, 43, 3920–3931; (c) Percec, V.; Grigoras, C. J Polym Sci Part A: Polym Chem 2005, 43, 5283–5299; (d) Percec, V.; Grigoras, C. J Polym Sci Part A: Polym Chem 2005, 43, 5609–5619; (e) Percec, V.; Barboiu, B.; Kim, H.-J. J Am Chem Soc 1998, 120, 305–316; (f) Percec, V.; Barboiu, B.; Grigoras, C.; Bera, T. K. J Am Chem Soc 2003, 125, 6503–6516.
29. Marutani, E.; Yamamoto, S.; Ninjbadgar, T.; Tjii, Y.; Fukuda, T.; Takano, M. Polymer 2004, 45, 2231–2235.
30. Wang, J.; Matyjaszewski, K. Macromolecules 1995, 28, 7901–7910.
31. Matsuno, R.; Yamamoto, K.; Otsuka, H.; Takahara, A. Chem Mater 2003, 15, 3–5.
32. Magonov, S. N.; Elings, V.; Whangbo, M.-H. Surf Sci 1997, 375, L385–L391.
33. Abbound, M.; Turner, M.; Duguet, E.; Fontanille, M. J Mater Chem 1997, 7, 1527–1532.
34. Jing, Z. Mater Lett 2006, 60, 2217–2221.
35. Wang, C.; Ro, S. Mater Chem Phys, in press.
36. Bartholome, C.; Beyou, E.; Bourgeat-Lami, E.; Chaumont, P.; Zydowicz, N. Macromolecules 2005, 38, 1099–1106.
37. Flesch, C.; Delaite, C.; Dumas, P.; Bourgeat-Lami, E.; Duguet, E. J Polym Sci Part A: Polym Chem 2004, 42, 6011–6020.
38. Advincula, R.; Ruehe, J,; Brittain, W.; Caster, K. Polymer Brushes; VCH-Wiley: Weinheim; 2004, Chapter 2, pp 51–68.
39. Matyjaszewski, K.; Kumar, A.; Tang, W. Macromolecules 2005, 38, 2015–2018.
40. Sumerlin, B. S.; Neugebauer, D.; Matyjaszewski, K. Macromolecules 2005, 38, 702–708.
41. Ohno, K.; Morinaga, T.; Koh, K.; Tsuji, Y.; Fukuda, T. Macromolecules 2005, 38, 2137–2142.
42. Pyun, J.; Jia, S.; Kowalewski, T.; Patterson, G. D.; Matyjaszewski, K. Macromolecules 2003, 36, 5094–5104.
43. Zhang, J.; Chen, P.; Sun, C.; Hu, X. Appl Catal A 2004, 266, 49–54.
44. Vesenka, J.; Manne, S.; Giberson, R.; Marsh, T.; Henderson, E. Biophys J 1993, 65, 992–997.
45. Fun, J.; Feng, X.; Han, Y.; Pan, C.; Yang, Y.; Li, B. Macromol Rapid Commun 2003, 24, 487–491.